

Modeling and inversion of PS-wave moveout asymmetry for tilted TI media: Part 2 — Dipping TTI layer

Pawan Dewangan¹ and Ilya Tsvankin²

ABSTRACT

Dipping transversely isotropic layers with a tilted symmetry axis (TTI media) cause serious imaging problems in fold-and-thrust belts and near salt domes. Here, we apply the modified PP + PS = SS method introduced in Part 1 to the inversion of long-offset PP and PS reflection data for the parameters of a TTI layer with the symmetry axis orthogonal to the bedding. The inversion algorithm combines the time- and offset-asymmetry attributes of the PSV-wave with the hyperbolic PP- and SS-wave moveout in the symmetry-axis plane (i.e., the vertical plane that contains the symmetry axis).

The weak-anisotropy approximations for the moveout-asymmetry attributes, verified by numerical analysis, indicate that small-offset (leading) terms do not contain independent information for the inversion. Therefore, the parameter-estimation algorithm relies on PS data recorded at large offsets (the offset-to-depth ratio has to reach at least two), which makes the results generally less stable than those for a horizontal TTI layer in Part 1. The least-resolved parameter is Thomsen's coefficient ϵ

that does not directly influence the moveout of either pure or converted modes.

Still, the contribution of the PS-wave asymmetry attributes helps to constrain the TTI model for large tilts ν of the symmetry axis ($\nu > 40^\circ$). The accuracy of the inversion for large tilts can be improved further by using wide-azimuth PP and PS reflections. With high-quality PS data, the inversion remains feasible for moderate tilts ($25^\circ < \nu < 40^\circ$), but it breaks down for models with smaller values of ν in which the moveout asymmetry is too weak. The tilt itself and several combinations of the medium parameters (e.g., the ratio of the P- and S-wave velocities in the symmetry direction), however, are well constrained for all symmetry-axis orientations.

The results of Parts 1 and 2 show that 2D measurements of the PS-wave asymmetry attributes can be used effectively in anisotropic velocity analysis for TTI media. In addition to providing an improved velocity model for imaging beneath TTI beds, our algorithms yield information for lithology discrimination and structural interpretation.

INTRODUCTION

Estimation of the parameters of tilted transversely isotropic (TTI) media is essential for anisotropic imaging beneath TTI formations and characterization of dipping fracture systems. Mode-converted PS-waves make a useful contribution in building TTI velocity models because of their high sensitivity to the anisotropic parameters.

In Part 1 (Dewangan and Tsvankin, 2006a), we proposed a modification of the PP + PS = SS method developed by Grechka and Tsvankin (2002) and Grechka and Dewangan (2003) for joint processing of PP and PS reflection data. In addition to the pseudoshear waves that possess the kinematics of pure SS primaries, our algorithm generates attributes of the moveout asymmetry of PS-waves. We also showed that the asymmetry attributes provide crucial infor-

mation needed to estimate the parameters of a horizontal TTI layer from surface PP and PS data.

The moveout of PS-waves becomes asymmetric if the traveltime does not stay the same when the source and receiver are interchanged. For a horizontal TTI layer (Part 1), the asymmetry is caused by the tilt of the symmetry axis. Another possible reason for the PS-wave moveout asymmetry is lateral heterogeneity in the form of lateral velocity variations or nonhorizontal reflectors. For example, PS moveout is asymmetric even in an isotropic or VTI (TI with a vertical symmetry axis) layer above a plane dipping reflector (Tsvankin and Grechka, 2000, 2002).

In active tectonic areas, originally horizontal TI layers are often rotated so that the symmetry axis remains orthogonal to the layer boundaries. Dipping shale layers of this type are commonly ob-

Manuscript received by the Editor July 19, 2004; revised manuscript received June 10, 2005; published online August 9, 2006.

¹Formerly Center for Wave Phenomena, Department of Geophysics, Colorado School of Mines, Golden, Colorado 80401; presently Geological Oceanography Division, National Institute of Oceanography, Dona Paula, Goa, India 403004. E-mail: pdewangan@darya.nio.org.

²Center for Wave Phenomena, Department of Geophysics, Colorado School of Mines, Golden, Colorado 80401. E-mail: ilya@dix.mines.edu.

© 2006 Society of Exploration Geophysicists. All rights reserved.

served in the fold-and-thrust region of the Canadian Foothills (e.g., Isaac and Lawton, 1999) and near salt domes (Tsvankin, 2001). Ignoring anisotropy in dipping TTI beds can cause significant mispositioning of reflection events in both vertical and horizontal directions (Isaac and Lawton, 1999; Vestrum et al., 1999; Lawton et al., 2001). Although migration algorithms can be readily extended to TTI media, accurate estimation of the required anisotropy parameters for imaging purposes remains a difficult problem.

The 2D inversion of P-wave normal-moveout (NMO) velocities for the parameters of dipping TTI layers with the symmetry axis perpendicular to the bedding was discussed by Grechka et al. (2001). Although their method performed well on full-waveform physical-modeling data, it is based on a number of simplifying assumptions about the model (e.g., the medium above the TTI layer has to be isotropic and homogeneous). Also, in addition to reflections from the TTI layer itself, the algorithm of Grechka et al. (2001) requires reflection data from a deeper horizontal interface. A review of several other velocity-analysis algorithms for TTI media (e.g., Grechka and Tsvankin, 2000) can be found in Part 1. It should be emphasized that if the dip and tilt of the symmetry axis are smaller than 40° , none of the existing methods can yield stable parameter estimates for a TTI layer using only PP and PS reflection data.

In this paper, we extend the methodology introduced in Part 1 to the inversion of multicomponent (PP and PSV) data acquired above a TTI layer with the symmetry axis orthogonal to the layer's bottom. The moveout asymmetry of PS-waves in this model is caused by both the reflector dip and the tilt of the symmetry axis, which are set equal to each other. The modified PP + PS = SS method yields the PSV-wave asymmetry attributes, which we combine in the inversion procedure with the NMO velocities, zero-offset traveltimes, and reflection time slopes of the pure PP and SS reflections.

The inversion algorithm is designed to estimate the P- and S-wave velocities in the symmetry direction (V_{p0} and V_{s0} , respectively), Thomsen (1986) anisotropy parameters ϵ and δ , the tilt ν , and the thickness of the layer using solely reflection traveltimes. We present simple analytic approximations for the time- and offset-asymmetry attributes of the PSV-wave and demonstrate that independent information for the inversion is contained in higher-order terms in offset, which become substantial as the offset-to-depth ratio approaches two. Numerical tests with the asymmetry attributes contaminated by Gaussian noise help to evaluate the stability of each parameter for a wide range of plausible TTI models. In combination with our layer-stripping technique (Dewangan and Tsvankin, 2006b), this inversion method can be applied to layered anisotropic media.

ASYMMETRIC PS-WAVE MOVEOUT IN A DIPPING TTI LAYER

For laterally heterogeneous models, such as a layer above a dipping reflector, the moveout of converted waves becomes asymmetric even in the absence of anisotropy (e.g., Tsvankin and Grechka, 2000). This asymmetry is commonly observed on split-spread common-midpoint gathers (CMP) in the offset domain because the traveltime does not stay the same when the source and receiver positions are interchanged. However, since these reciprocal traveltimes correspond to different reflection points, offset-domain measurements of the moveout asymmetry may be distorted by the influence of the reflector shape.

Moveout asymmetry from the PP + PS = SS method

An important advantage of estimating the asymmetry from the modified PP + PS = SS method is that each pair of the reciprocal PS events is guaranteed to have the same reflection point. Indeed, the method is designed to identify two PS-waves converted at the reflection point of a given PP-arrival (see Figure 1 in Part 1). Then the traveltimes of the SS-wave, which is not physically excited by the source, is obtained by combining the reflection times of the PP-wave and two PS-waves.

We consider a homogeneous TTI layer with the axis of symmetry orthogonal to the layer's bottom (reflector), which may have an arbitrary dip. Then the symmetry axis is confined to the dip plane of the reflector, which represents the only vertical symmetry plane of the model (we call it the *symmetry-axis plane*). The x_1 -axis of the Cartesian coordinate system points in the updip direction of the reflector (Appendix A).

According to Snell's law, the projection of the slowness vector onto the reflector should be the same for all reflected waves. If we denote the slowness components in the dip and strike directions of the reflecting interface by $p_{\text{int}1}$ and $p_{\text{int}2}$ (both $p_{\text{int}1}$ and $p_{\text{int}2}$ are confined to the reflector plane), the difference between the traveltimes of the two PS-waves with the same reflection point can be represented as

$$\Delta t_{PS} = t_{PS}(p_{\text{int}1}, p_{\text{int}2}) - t_{PS}(-p_{\text{int}1}, -p_{\text{int}2}) = \Delta t_P + \Delta t_S, \quad (1)$$

where Δt_P and Δt_S are the contributions to Δt_{PS} from the P- and S-legs of the PS ray, respectively. Equation 1 has the same form as the expression for Δt_{PS} in Part 1, where the slowness components are computed for a horizontal interface.

Following Part 1, we also define the measure of asymmetry in the offset \mathbf{x} (equation A-4) using the two PS-waves with the opposite signs of the slowness projection onto the reflector:

$$\Delta \mathbf{x}_{PS} = \mathbf{x}_{PS}(p_{\text{int}1}, p_{\text{int}2}) + \mathbf{x}_{PS}(-p_{\text{int}1}, -p_{\text{int}2}). \quad (2)$$

To gain insight into the influence of the model parameters on the time- and offset-asymmetry attributes, we analyze approximate expressions for Δt_{PS} and $\Delta \mathbf{x}_{PS}$ obtained in Appendices A and B under the assumption of weak anisotropy ($|\epsilon| \ll 1$ and $|\delta| \ll 1$) and small offset-to-depth ratio ($|p_{\text{int}1} V_{p0}| \ll 1$ and $|p_{\text{int}2} V_{p0}| \ll 1$). As shown in Appendix A, the approximate time-asymmetry attribute Δt_{PS} for the PSV-wave in the symmetry-axis plane (i.e., for the azimuth $\alpha = 0$) is given by

$$\Delta t_{PS} = \frac{-2 \sin \nu}{V_{s0}} \chi x_{SS} + \frac{(1 + 4\epsilon) V_{p0}^2 \sin \nu \cos^2 \nu}{4(1 + 2\sigma)^3 V_{s0}^3 z_d^2} x_{SS}^3, \quad (3)$$

where $\sigma \equiv (V_{p0}/V_{s0})^2(\epsilon - \delta)$, $\chi \equiv (\sigma - \delta)/(1 + 2\sigma)$, x_{SS} is the offset of the computed SS-wave, and z_d is the normal distance from the CMP to the reflector. The parameter χ was introduced by Grechka and Dewangan (2003) who showed that it can be obtained from the zero-offset traveltimes and NMO velocities of P- and SV-waves in layer-cake VTI media. Note that, although equation 3 is supposed to be linearized in the anisotropy parameters, the parameter σ was retained in the denominator of the x_{SS}^3 -term to increase the accuracy of the approximation (see Appendix A).

As expected, the asymmetry attribute Δt_{PS} vanishes for zero tilt and dip ($\nu = 0$) when the medium becomes VTI. Note that PS move-

out is asymmetric even in a dipping isotropic layer, where the cubic (equation 3) and higher-order terms in x_{SS} do not go to zero.

Figure 1 shows Δt_{PS} computed for a typical dipping TTI model from the exact equations 1 and A-1, as well as from the weak-anisotropy approximation (equation 3). While the initial slope of Δt_{PS} is well-described by the linear term in equation 3 even for large absolute values of δ and σ , the cubic and higher-order terms make a significant contribution at far offsets that correspond to offset-to-depth ratios of about two for the PP and PS data. Although the accuracy of the weak-anisotropy approximation decreases with offset, it correctly reproduces the trend of $\Delta t_{PS}(x_{SS})$ for moderate offset-to-depth ratios.

The weak-anisotropy approximation for the azimuthally varying offset-asymmetry attribute (equation 2) is derived in Appendix B. In the symmetry-axis plane ($\alpha = 0$), the approximate Δx_{PS} takes the following form:

$$\Delta x_{PS} = \frac{\sin \nu}{2z_d} \left[\frac{(1 + 4\delta)V_{P0}^2}{(1 + 4\sigma)V_{S0}^2} - 1 \right] x_{SS}^2. \quad (4)$$

Equation 4 indicates that for typical TI models with $\sigma \gg \delta$, the contribution of anisotropy reduces the offset-asymmetry attribute, which is confirmed by the numerical results in Figure 2. The weak-anisotropy approximation (equation 4) deteriorates with increasing offset because the exact solution is influenced by the quartic term in x_{SS} even for offset-to-depth ratios of the PS-wave close to two. For the moderately anisotropic model in Figure 2, the magnitude of Δx_{PS} reaches up to 50% of the CMP-to-reflector distance. However, the x_{SS}^3 -term in equation 4 does not contain independent information for estimating the model parameters.

Because of the influence of moveout asymmetry, the minimum traveltime of PS-wave on a CMP gather is not recorded at zero offset (Tsvankin and Grechka, 2000; Part 1). An analytic expression for the azimuthally-dependent offset $x_{\min}(\alpha)$ of the traveltime minimum is obtained in Appendix B by assuming a small dip ν and linearizing the exact equation in the anisotropy parameters. In the symmetry-axis plane, the approximation for x_{\min} reduces to

$$x_{\min}(\alpha = 0) = \frac{z_d}{2 \cos^2 \nu} \left[\frac{\sin \nu}{V_{P0}} - \frac{\sin \nu}{V_{S0}} \right] \times [V_{P0}(1 + 2\delta) + V_{S0}(1 + 2\sigma)]. \quad (5)$$

Although anisotropy does make a substantial contribution to $x_{\min}(\alpha = 0)$, all terms in equation 5 can be found from the NMO velocities, zero-offset traveltimes, and reflection time slopes of the pure (PP and SS) reflection modes (see below).

PARAMETER ESTIMATION

As discussed in Part 1, the main prerequisite for successful application of the inversion algorithm introduced here is acquisition of long-offset PP and PS data. First, offset-to-depth ratios of at least two for the recorded PP- and PS-waves are needed for stable estimation of the NMO velocity for the constructed SS arrivals. Second, acquiring PS data for a wide range of offsets ensures a sufficiently large magnitude of the moveout-asymmetry attributes used in the parameter estimation. Measurements of the asymmetry attributes at long offsets are particularly important in the inversion for a dipping TTI layer (see below).

Data processing

The data processing flow is similar to that described in Part 1. The PP + PS = SS method yields pseudoshear data, whose reflection moveout can be used to estimate the stacking (NMO) velocity ($V_{nmo,S}$), zero-offset traveltime (t_{S0}), and time slope on zero-offset section (i.e., the ray parameter p_{S0}) for the SS-waves (here, we operate only with SV-waves). The same parameters for the recorded PP-waves ($V_{nmo,P}$, t_{P0} , and p_{P0}) can be obtained from conventional hyperbolic semblance analysis. For wide-azimuth data, the NMO veloci-

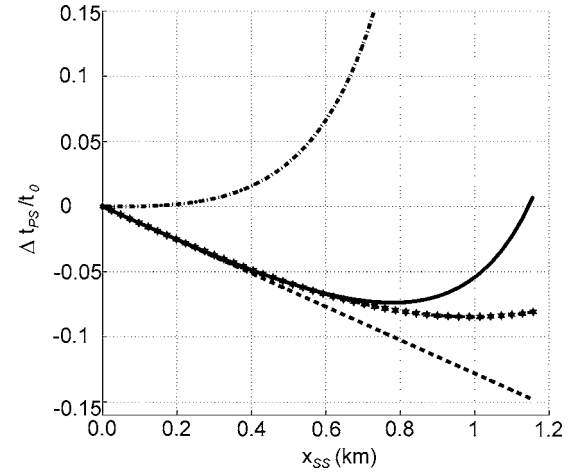


Figure 1. Time-asymmetry attribute Δt_{PS} for the PSV-wave in the symmetry-axis plane of a dipping TTI layer. The exact Δt_{PS} is marked by the solid line, the weak-anisotropy approximation (equation 3) by the dashed line with stars, the linear term in equation 3 by the dashed line, and Δt_{PS} in the reference isotropic model ($\epsilon = \delta = 0$) by the dash-dotted line. Δt_{PS} is normalized by the zero-offset traveltime of the PS-wave. The medium parameters are $V_{P0} = 4$ km/s, $V_{S0} = 2$ km/s, $\epsilon = 0.25$, $\delta = 0.1$, $\nu = 25^\circ$, and $z_d = 1$ km. The maximum offset-to-depth ratio of the input PP and PS data is close to two.

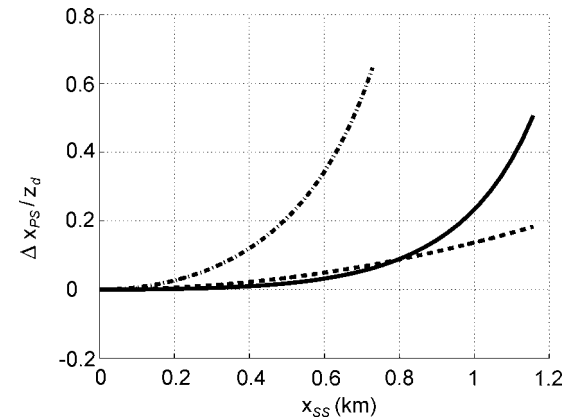


Figure 2. Offset-asymmetry attribute Δx_{PS} for the PSV-wave in the symmetry-axis plane. The exact Δx_{PS} is marked by the solid line, the weak-anisotropy approximation 4 by the dashed line, and Δx_{PS} in the reference isotropic model by the dash-dotted line. Δx_{PS} is normalized by the distance z_d between the CMP and the reflector. The medium parameters are the same as those in Figure 1.

ties of the PP- and SS-waves are replaced by the NMO ellipses determined from azimuthal moveout analysis (Grechka and Tsvankin, 1999; Part 1).

Then we combine the moveout parameters of the pure PP and SS reflections with the two PS-wave asymmetry attributes obtained from a modified PP + PS = SS method: Δt_{PS} (equations 1 and 3) and Δx_{PS} (equations 2 and 4). The offset x_{\min} (equation 5) that was used in Part 1 does not contain any additional information about the model and, therefore, is not included in the inversion.

Inversion algorithm

Suppose that both PP and PS (PSV) reflection data are acquired in a 3D survey for a wide range of azimuths, and the PP + PS = SS method is used to generate pseudoshear reflections and the asymmetry attributes of the PSV-wave³. The orientation of the symmetry-axis is plane can be established from the NMO ellipses of the pure modes, whose axes are aligned with the dip and strike directions of the re-

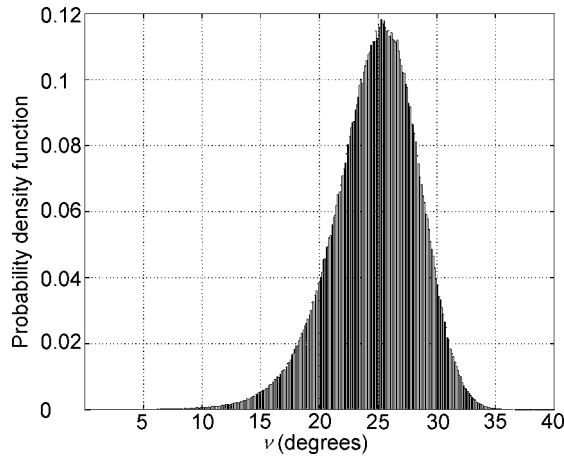


Figure 3. Probability density function of the tilt ν computed from equation 6 assuming a 2% error in the NMO velocities. The model parameters are the same as those in Figure 1.

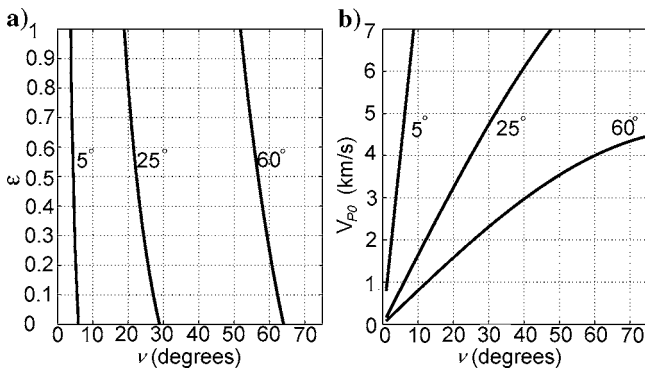


Figure 4. Range of possible solutions for the parameters (a) ϵ and (b) V_{P0} obtained from PP- and SS-waves in the symmetry-axis plane by scanning over the tilt ν . All model parameters except for the tilt ($\nu = 5^\circ, 25^\circ,$ and 60°) are the same as those in Figure 1 ($\epsilon = 0.25, V_{P0} = 4$ km/s).

flector. Processing of the PP-waves yields the semi-axes of the P-wave NMO ellipse ($V_{\text{nmo,P}}^{\text{dip}}$ and $V_{\text{nmo,P}}^{\text{strike}}$), zero-offset traveltime, and time slope on the zero-offset section:

$$V_{\text{nmo,P}}^{\text{dip}} = \frac{V_{P0} \sqrt{1 + 2\delta}}{\cos \nu}, \quad V_{\text{nmo,P}}^{\text{strike}} = V_{P0} \sqrt{1 + 2\delta}, \quad (6)$$

$$t_{P0} = \frac{z_d}{V_{P0}}, \quad (7)$$

$$p_{P0} = \frac{\sin \nu}{V_{P0}}. \quad (8)$$

The velocity $V_{\text{nmo,P}}^{\text{dip}}$ for the TTI model with the symmetry axis orthogonal to the reflector is derived in Tsvankin (1995, 2001); we found the strike component of the NMO ellipse in a similar way. The expressions for t_{P0} and p_{P0} are obtained using the fact that the zero-offset ray in our model is parallel to the symmetry axis.

The corresponding attributes for the SS-wave can be estimated from the computed SS data:

$$V_{\text{nmo,S}}^{\text{dip}} = \frac{V_{S0} \sqrt{1 + 2\sigma}}{\cos \nu}, \quad V_{\text{nmo,S}}^{\text{strike}} = V_{S0} \sqrt{1 + 2\sigma}, \quad (9)$$

$$t_{S0} = \frac{z_d}{V_{S0}}, \quad (10)$$

$$p_{S0} = \frac{\sin \nu}{V_{S0}}. \quad (11)$$

The model vector for the TTI layer includes the following components:

$$\mathbf{m} \equiv \{V_{P0}, V_{S0}, \epsilon, \delta, \nu, z_d\}, \quad (12)$$

where the tilt ν of the symmetry axis is taken to be equal to the reflector dip. For noise-free data, all six model parameters can be recovered uniquely using the NMO velocities, zero-offset traveltimes, and zero-offset time slopes of the PP- and SS-waves. Indeed, the tilt ν can be found from the ratio of the NMO velocities of either wave in the dip and strike directions, which allows us to obtain the vertical velocities V_{P0} and V_{S0} from the ray parameters p_{P0} and p_{S0} . Finally, the distance z_d and parameters ϵ and δ can be inferred from the zero-offset times and NMO ellipses. However, in the presence of noise, estimation of the tilt from the ratio of the NMO velocities is highly unstable for small and moderate values of ν .

This instability can be illustrated by computing the range of possible tilt values for the NMO velocities contaminated by Gaussian noise with a standard deviation of 2% (Figure 3). The estimation of tilt is unbiased with the distribution centered at the correct value ($\nu = 25^\circ$), and has a standard deviation close to 3.5° . According to the sensitivity plots in Figure 4 (this plot is discussed in detail below), such a scatter in ν is sufficient to cause unacceptably large errors in the parameters ϵ and V_{P0} . Thus, a realistic distortion of 1-2% in the NMO velocities propagates with a significant amplification into the other parameters. This conclusion is also supported by the results of Grechka et al. (2002), who found the inversion of the PP and SS (SVSV) NMO ellipses, zero-offset times, and reflection time slopes in a dipping TTI layer to be nonunique for tilts and dips smaller than $30\text{--}40^\circ$.

³As in Part 1, SV-wave is the shear wave polarized in the plane formed by the slowness vector and the symmetry axis.

It is important for practical applications to study the inverse problem for the common case when only 2D data in the symmetry-axis plane are available. The pure-mode data vector in this case has six elements ($V_{\text{nmo,P}}^{\text{dip}}, t_{P0}, p_{P0}, V_{\text{nmo,S}}^{\text{dip}}, t_{S0}$, and p_{S0}) but only five of them are independent because of the constraint,

$$\frac{p_{S0}}{p_{P0}} = \frac{t_{S0}}{t_{P0}}. \quad (13)$$

Since the model vector (equation 12) has six parameters, 2D inversion cannot be carried out without additional information, such as the asymmetry attributes of the PS-wave. The results of the previous section, however, indicate that the leading terms in the expressions for asymmetry attributes depend on just the moveout parameters of the pure (PP and SS) modes. Indeed, rewriting equations 3–5 in terms of the NMO velocities, zero-offset times, and reflection time slopes of the PP- and SS-waves, we find (only the linear term in equation 3 is included)

$$\Delta t_{PS} = p_{S0} \left(\frac{V_{\text{nmo,P}}^2 t_{P0}^2}{V_{\text{nmo,S}}^2 t_{S0}^2} - 1 \right) x_{SS}, \quad (14)$$

$$\Delta x_{PS} = \frac{p_{S0}}{2t_{S0}} \left(\frac{V_{\text{nmo,P}}^4 t_{P0}^2}{V_{\text{nmo,S}}^4 t_{S0}^2} - 1 \right) x_{SS}^2, \quad (15)$$

$$x_{\min} = \frac{t_{S0}}{2p_{S0}} (p_{P0} - p_{S0}) (V_{\text{nmo,P}}^2 p_{P0} + V_{\text{nmo,S}}^2 p_{S0}). \quad (16)$$

All NMO velocities in equations 14–16 are the dip components of the NMO ellipses measured in the symmetry-axis plane.

Clearly, only the departure of the exact asymmetry attributes from the small-offset approximations (equations 14–16) can provide independent information for the parameter estimation. As illustrated by Figures 1 and 2, such departures for both the time- and offset-asymmetry attributes become substantial when the offset-to-depth ratio for the recorded PP and PS data approaches two.

We propose the following algorithm to invert the 2D multicomponent data in the symmetry-axis plane for the model vector (equation 12):

- For each value of the tilt ν from 0° to 90° , find the model vector from the parameters $V_{\text{nmo,P}}^{\text{dip}}, t_{P0}, p_{P0}, V_{\text{nmo,S}}^{\text{dip}}, t_{S0}$, and p_{S0} (equations 6–11). Restrict the range of plausible tilts by putting reasonable constraints on the parameter ϵ ($0 \leq \epsilon \leq 1$; see Figure 4).
- Taking into account errors in the measured quantities, compute the range of models that fit the pure-mode data within the noise level for each plausible tilt.
- For each model found in the previous step, compute the asymmetry attributes from the exact equations 1 and 2.
- Calculate the following misfit function for the asymmetry attributes over the full range of offsets (the maximum offset-to-depth ratio of the PP and PS data should be no smaller than two):

$$\mathcal{F} \equiv \frac{\sum (\Delta t_{PS}^{\text{calc}} - \Delta t_{PS}^{\text{meas}})^2}{(\sum \Delta t_{PS}^{\text{meas}})^2} + \frac{\sum (\Delta x_{PS}^{\text{calc}} - \Delta x_{PS}^{\text{meas}})^2}{(\sum \Delta x_{PS}^{\text{meas}})^2}. \quad (17)$$

- Identify the model vector that minimizes the misfit function.

Prior to applying the inversion algorithm, we present the sensitivity analysis for noise-free data. For the test in Figure 4, we computed the NMO velocities, zero-offset traveltimes, and reflection time slopes for the PP- and SS-waves from the exact equations for three different values of the tilt ν . Then, for each of the three models we scanned over tilt and computed the model parameters from equations 6–11, as described above. It is clear from Figure 4a that the parameter ϵ is highly sensitive to ν , and only a narrow range of tilts produces plausible ϵ values within the interval $0 \leq \epsilon \leq 1$. The variation of the parameter ϵ with ν is particularly rapid for small tilts corresponding to models approaching VTI. Therefore, putting reasonable constraints on ϵ helps to reduce substantially the range of ν for which we need to compute the asymmetry attributes at the second stage of the inversion procedure.

According to Figure 4a, small errors in ν may produce large distortions in estimated ϵ , especially for mild tilts. The problem in resolving ϵ is related to the fact that it contributes to the data vector only indirectly, through the parameter σ (equations 6–11). Both σ and δ are more tightly constrained by the input data than is ϵ (see below), with the exception of quasi-VTI models with small ν , for which the inversion as a whole breaks down. In contrast to ϵ , the vertical velocity V_{p0} is much less sensitive to the tilt, especially for moderate and large values of ν (Figure 4b). The dependence of the parameters V_{S0} and z_d on ν shows a pattern similar to that for V_{p0} .

To identify the true model from the range of models that fit the pure-mode data, we use the time- and offset-asymmetry attributes in the symmetry-axis plane. Figure 5 displays the square-root of the objective (misfit) function (equation 17), which is equivalent to the standard deviation of the error in each of the asymmetry attributes. The expected value of the misfit function can be represented as

$$\begin{aligned} E[\mathcal{F}] &= E \left[\frac{\{\mathbf{x} - (\mathbf{x} + \xi\mathbf{x})\} \cdot \{\mathbf{x} - (\mathbf{x} + \xi\mathbf{x})\}}{\mathbf{x} \cdot \mathbf{x}} \right] \\ &= E[\xi^2] = \beta_\xi^2 + (E[\xi])^2 = \beta_\xi^2, \end{aligned}$$

where ξ is a random variable with zero mean and standard deviation β_ξ , and \mathbf{x} is the vector of either the time- or offset-asymmetry values for different offsets.

For noise-free data, all model parameters can be estimated uniquely because the misfit function for both Δt_{PS} and Δx_{PS} goes to zero at the correct tilt angle (Figure 5). In the presence of noise, the

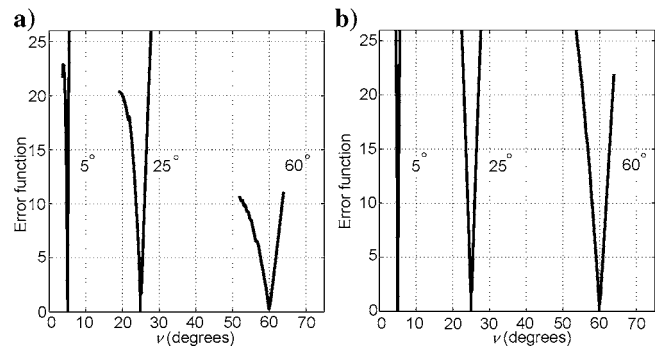


Figure 5. Square root of the misfit function equation 17 for (a) the time-asymmetry attribute Δt_{PS} ; and (b) the offset-asymmetry attribute Δx_{PS} . The misfit function is computed for the models in Figure 4 which fit the pure-mode data and satisfy the constraint $0 \leq \epsilon \leq 1$.

resolution in tilt becomes lower for larger values of ν where the misfit function increases more slowly away from the correct solution. This result is supported by equation 3 for the time-asymmetry attribute Δt_{PS} in which the ratio of the cubic and linear terms in offset decreases with ν . As discussed above, only the cubic and higher-order terms in the equation for Δt_{PS} contain independent information for the inversion.

Note that the high resolution in ν for quasi-VTI models with mild tilt does not mean that the rest of the parameters can be estimated with high accuracy. Despite the tight constraints on the tilt provided by both the pure-mode signatures and the asymmetry attributes, not only ϵ , but also δ and the vertical velocities are too sensitive to tilt for the inversion to be sufficiently stable (see the numerical results below).

Figure 5 also shows that the time- and offset-asymmetry attributes provide comparable resolution in tilt, although Δx_{PS} performs somewhat better than Δt_{PS} for relatively large tilts and also for large errors in the asymmetry attributes. Therefore, the inversion algorithm employs equation 17 with equal weights for Δt_{PS} and Δx_{PS} .

Numerical examples

To evaluate the stability of the parameter estimation, we present a series of numerical tests in which the input data were computed from the exact equations and contaminated by Gaussian noise. For each

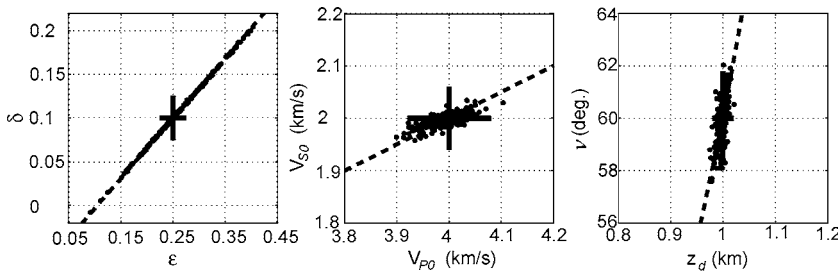


Figure 6. Inverted parameters (dots) of a dipping TTI layer with $\nu = 60^\circ$ obtained from 2D PP and PS data in the symmetry-axis plane. The correct model parameters are marked by the crosses. The dashed lines on the $[\epsilon, \delta]$, $[V_{P0}, V_{S0}]$, and $[\nu, z_d]$ plots correspond to the correct values of χ , V_{P0}/V_{S0} , and $\sin \nu/z_d$, respectively. The input data were contaminated by Gaussian noise with the standard deviations of 2% for the NMO velocities, 0.5% for the zero-offset traveltimes, 1% for the time slopes, and 2% for the PS-wave asymmetry attributes.

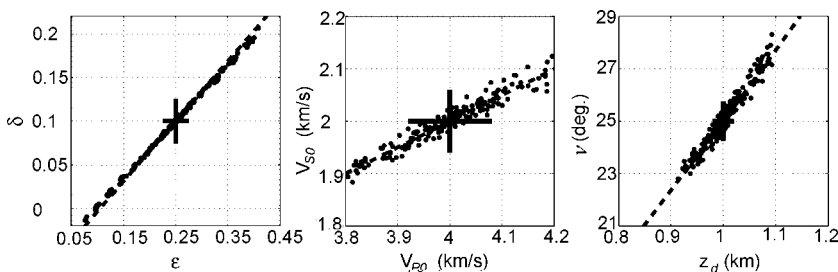


Figure 7. Inversion results for a model with same parameters as those in Figure 6 except for the tilt $\nu = 25^\circ$. The dashed lines on the $[\epsilon, \delta]$, $[V_{P0}, V_{S0}]$, and $[\nu, z_d]$ plots correspond to the correct values of χ , V_{P0}/V_{S0} , and $\sin \nu/z_d$, respectively. The standard deviations in the asymmetry attributes are increased to 6%; the deviations in the NMO velocities (2%), zero-offset traveltimes (0.5%), and time slopes (1%) remain the same.

model, the parameter vector \mathbf{m} (equation 12) is obtained for 200 realizations of the input data using the inversion algorithm described above.

In the previous section, we showed that the leading terms in the offset x_{SS} in the equations for the asymmetry attributes do not provide independent information for the parameter estimation. Therefore, to assess the accuracy of the inversion, it is convenient to define the “nonlinearity factor” for the time asymmetry Δt_{PS} as

$$NL \equiv \max \left\{ \frac{|\Delta t_{PS}^{\text{lin}} - \Delta t_{PS}^{\text{exact}}|}{|\Delta t_{PS}^{\text{lin}}|} \right\}, \quad (18)$$

where $\Delta t_{PS}^{\text{exact}}$ is the exact value and $\Delta t_{PS}^{\text{lin}}$ is the linear term in x_{SS} (equation 3); NL is computed for the maximum PS-wave offset-to-depth ratio equal to two. Since the sensitivity of the offset-asymmetry attribute to the model parameters is similar to that for the time asymmetry (see Figure 5), we do not include Δx_{PS} in equation 18. If the nonlinearity factor is large (close to or greater than unity, according to our estimates), nonlinear terms in Δt_{PS} are substantial and the asymmetry attributes typically provide significant independent information for the inversion.

First, we consider TTI media with large tilts of the symmetry axis ($\nu > 40^\circ$), which also implies steep dips. Such models are typical for the Rocky Mountain Foothills in Western Canada and other fold-and-thrust belts that contain steeply dipping TI shale layers (e.g., Isaac and Lawton, 1999).

The inversion for $\nu = 60^\circ$ produces unbiased results, with the mean of each model parameter close to the correct value (Figure 6). Whereas the nonlinearity factor for the model in Figure 6 is smaller than unity ($NL = 0.6$), the moveout asymmetry is quite pronounced, with the maximum of Δt_{PS} reaching 20% of the zero-offset PS traveltime, and the maximum of Δx_{PS} at far offsets reaching 70% of z_d . In comparison, for the reference isotropic medium with $\epsilon = \delta = 0$, the nonlinearity factor is infinite, the maximum of Δt_{PS} is also 20% of the zero-offset time, and Δx_{PS} is up to 110% of z_d . Since the magnitude of the asymmetry attributes is relatively large, it should be possible to estimate both Δt_{PS} and Δx_{PS} with high accuracy.

If we assume that the error in the asymmetry attributes is 2%, the parameters V_{P0} , V_{S0} , and z_d are well constrained (the standard deviation is less than 1%), and the standard deviation in ν is only 1° (Figure 6). In agreement with the relatively small value of the nonlinearity factor, however, the inverted anisotropic parameters ϵ and δ exhibit more scatter, with the standard deviation reaching 0.06 and 0.04, respectively. Also, the estimates of ϵ and δ degrade rapidly as the error in the asymmetry attributes increases, while the deviations in V_{P0} , V_{S0} , and z_d remain small. It is clear from Figure 6 that the best-constrained parameter combinations are $\chi \equiv (\sigma - \delta)/(1 + 2\sigma)$, $\sin \nu/z_d$, and V_{P0}/V_{S0} . In principle, ϵ and δ for large tilts can be obtained with sufficient accuracy from wide-azimuth PP and SS data, as demonstrated by Grechka et al. (2002).

If the tilt for the model from Figure 6 is reduced from 60° to 25° (Figure 7), the nonlinearity factor increases to 1.1, which indicates that for the same errors in the input data the inversion should become more stable (i.e., the model parameters should be better resolved). The magnitude of Δt_{PS} for $\nu = 25^\circ$, however, decreases to just 8% of zero-offset time (the corresponding value for the reference isotropic medium is 14%). Therefore, we expect the uncertainty in the Δt_{PS} and Δx_{PS} to become larger for mild tilts.

If the error in the asymmetry attributes is set to 6%, the standard deviation of the tilt ν is almost the same (1°) as that in Figure 6. Despite the high resolution in ν , Figure 7 shows that the standard deviations in V_{P0} , V_{S0} , and z_d increase to about 4%; the deviations in ϵ and δ are also substantial (0.08 and 0.05, respectively). Although the accuracy in all model parameters becomes much higher if the error in the asymmetry attributes is limited to 2%, the small magnitude of Δt_{PS} and Δx_{PS} makes such low error levels unrealistic.

An interesting special case is that of an elliptically anisotropic medium ($\epsilon = \delta$). For the same tilt $\nu = 25^\circ$ as that in Figure 7, but with $\epsilon = \delta = 0.2$, the nonlinearity factor $NL = 2.1$, which indicates a large contribution of the higher-order terms in offset in the equations for Δt_{PS} and Δx_{PS} . The magnitude of the time-asymmetry attribute is also substantial (about 20% of zero-offset time), so the inversion should be stable. It turns out, however, that the parameter estimation is feasible only if the elliptical condition is assumed in advance (i.e., the inversion is performed with $\epsilon = \delta$). If the inversion is carried out without any assumption about ϵ and δ , several model parameters exhibit large scatter, even though the tilt is well-constrained.

To understand the influence of the asymmetry error on the inverted parameters, we repeated the inversion for a wide range of the standard deviations in Δt_{PS} and Δx_{PS} (Figures 8 and 9). Figure 8 shows that for the same-size errors in the input data, the velocity V_{P0} becomes better constrained for models with larger tilt, whereas for ν the opposite is true. The results for V_{P0} are explained by the much lower sensitivity of this parameter to distortions in tilt for models with large values of ν (Figure 4b). The standard deviations in the shear-wave velocity V_{S0} and the distance z_d are close to those for V_{P0} .

Overall, the tilt remains well resolved for errors in the asymmetry attributes of up to at least 15% (Figure 8b). The accuracy in the parameters V_{P0} , V_{S0} , and z_d , however, is acceptable only for large tilts over 40° (Figure 8a). For moderate values of ν , between 25° and 40° , V_{P0} , V_{S0} , and z_d can be constrained using good-quality converted-wave data that produce small errors in the asymmetry attributes. If the tilt is smaller than 25° , the moveout asymmetry is weak, and the large uncertainty in Δt_{PS} and Δx_{PS} should make the estimates of V_{P0} , V_{S0} , and z_d highly inaccurate.

The standard deviations in the parameters ϵ and δ (Figure 9) show a pattern similar to that for the tilt (Figure 8b). For the same level of the asymmetry errors, both ϵ and δ are better resolved for smaller values of ν . The error curves in

Figure 9a and 9b have almost the same shape for all ν because the parameter χ , which is well constrained by the data, is close to a linear combination of ϵ and δ . However, because ϵ does not directly contribute to the vector of input data, its standard deviation is about 50% larger (on average) than the deviation in δ . Given the expected decrease of the asymmetry errors with tilt, the errors in ϵ and δ should be almost constant for a wide range of moderate and large tilts and rapidly increase for quasi-VTI models with small values of ν .

If wide-azimuth PP and PS data are available, we can design a similar inversion algorithm by combining the NMO ellipses, zero-offset traveltimes, and time slopes of the pure modes with the 3D asymmetry attributes of the PSV-wave. Linearization of equations A-26 and B-8 for small tilts ν shows, however, that the variation of the asymmetry attributes with azimuth α can be predicted from their dip components ($\alpha = 0$):

$$\Delta t_{PS}(\alpha) = \Delta t_{PS}(0) \cos \alpha, \quad (19)$$

$$\Delta x_{PS}(\alpha) = \Delta x_{PS}(0) \cos \alpha. \quad (20)$$

Hence, the magnitude of the asymmetry attributes decreases away from the dip direction and goes to zero in the $[x_2, x_3]$ -plane. The

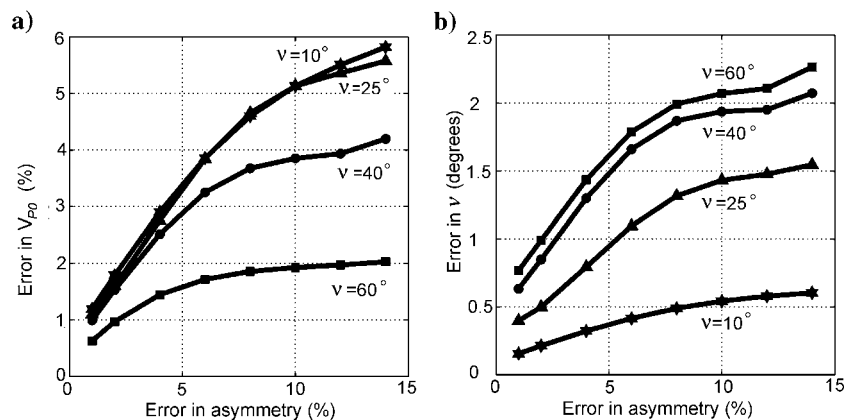


Figure 8. Error (the standard deviation) in (a) the velocity V_{P0} and (b) the tilt ν as a function of the standard deviation in the asymmetry attributes. The tilts are 10° (the line with stars), 25° (triangles), 40° (circles), and 60° (squares). The parameters V_{P0} , V_{S0} , ϵ , δ , and z_d and the standard deviations in the NMO velocities, zero-offset times, and time slopes are the same as those in Figure 6.

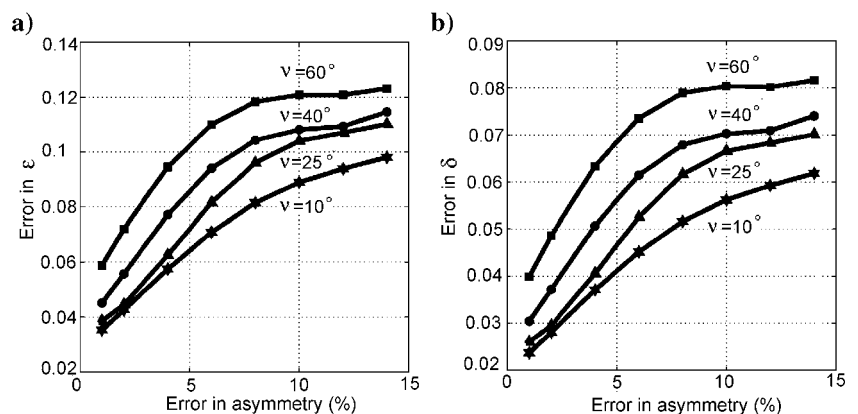


Figure 9. Same as Figure 8, but the error is computed for the parameters (a) ϵ and (b) δ .

weakened moveout asymmetry for azimuths away from the dip direction means that including the azimuthal variation of Δt_{PS} and Δx_{PS} can increase the signal-to-noise ratio only marginally. An alternative or complementary option for enhancing the signal is summation (stacking) of the dip components of the asymmetry attributes for adjacent CMP locations under the assumption of weak lateral heterogeneity.

For large tilts ($\nu > 40^\circ$), the azimuthal variation of the moveout attributes becomes more complicated and cannot be described by equations 19 and 20. Numerical testing (not included here) indicates that if $\nu > 40^\circ$, the factors $\Delta t_{PS}(\alpha)$ and $\Delta x_{PS}(\alpha)$ measured in wide-azimuth surveys provide useful constraints on the model parameters. However, for wide-azimuth data acquired over TTI layers with large tilts (dips), the asymmetry attributes are redundant because the inversion can be carried out using PP and SS data alone (Grechka et al., 2002).

CONCLUSIONS

The modified PP + PS = SS method is applied here to the inversion of multicomponent (PP and PSV) data acquired over a dipping TTI layer with the symmetry axis orthogonal to the layer's bottom. As is the case for a horizontal TTI layer, the moveout asymmetry attributes of the PSV-wave play a crucial role in the parameter-estimation procedure.

To analyze the moveout asymmetry in the vertical plane that contains the symmetry axis (the symmetry-axis plane), we developed weak-anisotropy, small-offset approximations for the time- and offset-asymmetry attributes (Δt_{PS} and Δx_{PS}). Although the anisotropy has a strong influence on both Δt_{PS} and Δx_{PS} even at small offsets, the leading terms in offset depend just on the moveout parameters of the pure (PP and SS) reflection modes. Therefore, independent information for the inversion procedure is contained only in the higher-order terms in offset that become significant when the offset-to-depth ratio for the PS-waves approaches two.

It should be emphasized that 2D moveout inversion of just pure-mode (PP and SS) data in the symmetry-axis plane is nonunique, and even 3D inversion breaks down for small and moderate tilts ν of the symmetry axis. The addition of the PS-wave asymmetry attributes to the NMO velocities, zero-offset traveltimes, and reflection time slopes of the recorded PP-waves and the constructed SS-waves can help to invert 2D data in the symmetry-axis plane without a priori information. The inversion algorithm is designed as a two-stage procedure, with the attributes Δt_{PS} and Δx_{PS} computed only for the family of plausible models, which fit the pure-mode data.

To predict the stability of the inversion for a given TTI model, we introduce the nonlinearity factor (NL) which quantifies the relative magnitude of the cubic and higher-order terms in offset for the time asymmetry Δt_{PS} . Relatively small values $NL < 1$, which result in part from limited offset range of the acquired PP and PS data, typically indicate that the estimated parameters are highly sensitive to noise.

Application of the algorithm to noise-contaminated input data shows that the tilt ν of the symmetry axis is well resolved even when the model approaches VTI ($\nu = 0^\circ$). The accuracy in the symmetry-direction velocities V_{P0} and V_{S0} and the distance z_d from the CMP to the reflector is sufficient only if the symmetry axis deviates by at least 25° from the vertical. For moderate tilts $25^\circ < \nu < 40^\circ$, however, the inversion for V_{P0} , V_{S0} , and z_d is possible only if the errors in the asymmetry attributes are relatively small (i.e., for high-quality

data). The resolution in the anisotropy parameters ϵ and δ is flat over a wide range of moderate and large tilts, with δ constrained much tighter than ϵ . For quasi-VTI models with $\nu < 15\text{--}20^\circ$, the magnitude of the asymmetry attributes is insufficient for reliable estimation of all model parameters, except for the tilt itself. Our analysis shows that the best-constrained parameter combinations over a wide range of tilts are $\chi \equiv (\sigma - \delta)/(1 + 2\sigma)$, $\sin \nu/z_d$, and V_{P0}/V_{S0} .

On the whole, the 2D inversion in the symmetry-axis plane gives acceptable results if the tilt exceeds 40° and, for high-quality input PS data, for the range of moderate tilts $25^\circ < \nu < 40^\circ$. Still, the accuracy of the inverted parameter ϵ is marginal even for large values of ν (i.e., for large tilts and dips). Note that the inversion for $\nu > 40^\circ$ can be accomplished even without the asymmetry information, but it requires wide-azimuth PP and PS (or PP and SS) data. The addition of wide-azimuth data (including the asymmetry attributes), however, does not help in the parameter estimation for moderate tilts.

The inversion algorithm developed here can help in building TTI velocity models in depth from multicomponent reflection data. Taking tilted transverse isotropy in dipping layers into account is particularly important in fold-and-thrust belts (such as the Canadian Foot-hills) and near salt domes.

ACKNOWLEDGMENTS

We are grateful to members of the A(nisotropy)-Team of the Center for Wave Phenomena (CWP), Colorado School of Mines (CSM), for helpful discussions. Careful reviews by Ken Larner (CSM) and the editors and referees of GEOPHYSICS helped to improve the manuscript. The support for this work was provided by the Consortium Project on Seismic Inverse Methods for Complex Structures at CWP and by the Chemical Sciences, Geosciences and Biosciences Division, Office of Basic Energy Sciences, Office of Science, U. S. Department of Energy.

APPENDIX A

APPROXIMATE TIME-ASYMMETRY ATTRIBUTE FOR THE PSV-WAVE

To derive explicit expressions for the PSV-wave time- and offset-asymmetry attributes in a TTI layer, we use the exact parametric representation of converted-wave moveout developed in Tsvankin (2001, Chapter 5) and Tsvankin and Grechka (2002). The PS-wave reflection traveltime in a homogeneous layer above a plane dipping reflector can be found in the following form:

$$t_{PS} \equiv t_P + t_S = z_r(q_P - p_{1P}q_{1P} - p_{2P}q_{2P} + q_S - p_{1S}q_{1S} - p_{2S}q_{2S}), \quad (\text{A-1})$$

where t_P and t_S are the traveltimes along the P- and S-legs, respectively; z_r is the depth of the conversion point at the reflector; p_1 and p_2 are the horizontal components of the slowness vector (the subscripts P and S indicate the wave type); $q \equiv p_3$ is the vertical slowness; and $q_i \equiv \partial q / \partial p_i$ ($i = 1, 2$). The depth of the conversion point can be represented in terms of the vertical distance z_{CMP} from the CMP to the reflector:

$$z_r = \frac{z_{\text{CMP}}}{1 + \Delta z}, \quad (\text{A-2})$$

$$\Delta z = \frac{\tan \phi}{2} [(q_{,1P} + q_{,1S})\zeta_1 + (q_{,2P} + q_{,2S})\zeta_2]. \quad (\text{A-3})$$

Here $\{\zeta_1, \zeta_2\}$ is a horizontal unit vector in the updip direction and ϕ is the reflector dip.

The source-receiver offset x_{PS} of the PS-wave and the azimuth α of the source-receiver line with respect to the x_1 -axis can be written as

$$x_{PS} = |\mathbf{x}_{PS}| = \sqrt{x_1^2 + x_2^2}, \quad (\text{A-4})$$

$$\alpha = \tan^{-1}\left(\frac{x_2}{x_1}\right), \quad (\text{A-5})$$

where x_1 and x_2 are the components of the source-receiver vector \mathbf{x}_{PS} :

$$x_1 = z_r(q_{,1P} - q_{,1S}), \quad (\text{A-6})$$

$$x_2 = z_r(q_{,2P} - q_{,2S}). \quad (\text{A-7})$$

A detailed derivation of equations A-1–A-7 can be found also in Tsvankin (2001, Appendix 5E).

For a weakly anisotropic TTI layer ($|\epsilon| \ll 1$ and $|\delta| \ll 1$), the asymmetry attribute Δt_{PS} obtained from the PP + PS = SS method (equations 1 and 2) can be linearized in the anisotropic coefficients ϵ and δ under the additional assumption of small offset x_{PS} . Here, we consider a TTI layer with the tilt of the symmetry axis equal to the reflector dip (Figure A-1). Since the PP + PS = SS method operates with the PP and PS arrivals that have the same reflection point, Snell's law dictates that the projection of the slowness vector onto the reflector is identical (in absolute value) for all reflected waves.

Using simple trigonometric relationships, the slowness components for the incident and reflected P-waves can be written as

$$p_{i1} = p_{\text{int}1} \cos \nu + q^{\text{VTI}} \sin \nu, \quad (\text{A-8})$$

$$p_{r1} = -p_{\text{int}1} \cos \nu + q^{\text{VTI}} \sin \nu, \quad (\text{A-9})$$

$$p_{i2} = p_{\text{int}2} = -p_{r2}, \quad (\text{A-10})$$

where $p_{\text{int}1}$ and $p_{\text{int}2}$ are the slowness components of the incident and reflected waves along the interface in the dip and strike directions, respectively; q^{VTI} is the slowness component in the symmetry-axis direction; p_{i1} and p_{r1} are the horizontal slownesses of the incident and the reflected waves in the symmetry-axis (dip) plane (Figure A-1); and p_{i2} and p_{r2} are the slowness components of the incidence and reflected waves in the strike direction. The above relationships between the slownesses remain valid for the S-wave as well.

In the weak-anisotropy approximation, q^{VTI} can be expressed in terms of $p_{\text{int}1}$ and $p_{\text{int}2}$ using the VTI equations for P-waves (Tsvankin and Grechka, 2000):

$$q^{\text{VTI}} = q_{P0} \left\{ 1 - \frac{(p_{\text{int}1}^2 + p_{\text{int}2}^2)}{q_{P0}^2} \times [\delta + (\epsilon - \delta)(p_{\text{int}1}^2 + p_{\text{int}2}^2)V_{P0}^2] \right\}, \quad (\text{A-11})$$

$$q_{P0} = \sqrt{\frac{1}{V_{P0}^2} - (p_{\text{int}1}^2 + p_{\text{int}2}^2)}. \quad (\text{A-12})$$

Substituting the approximate q^{VTI} from equation A-11 into equations A-8 and A-9 and linearizing the resulting expressions for small off-set-to-depth ratio ($|p_{\text{int}1}V_{P0}| \ll 1$, $|p_{\text{int}2}V_{P0}| \ll 1$), we obtain

$$p_{i1} = \frac{\sin \nu}{V_{P0}} + p_{\text{int}1} \cos \nu - \frac{(p_{\text{int}1}^2 + p_{\text{int}2}^2)V_{P0} \sin \nu(1 + 2\delta)}{2}, \quad (\text{A-13})$$

$$p_{r1} = \frac{\sin \nu}{V_{P0}} - p_{\text{int}1} \cos \nu - \frac{(p_{\text{int}1}^2 + p_{\text{int}2}^2)V_{P0} \sin \nu(1 + 2\delta)}{2}. \quad (\text{A-14})$$

The linearized equation for the vertical slowness components q and their partial derivatives $q_{,i} \equiv \partial q / \partial p_i$ ($i = 1, 2$) are derived from p_{i1} and p_{r1} following the procedure discussed in Part 1.

If the asymmetry attributes are computed on a line with a fixed azimuth α , the relationship between $p_{\text{int}1}$ and $p_{\text{int}2}$ can be obtained by linearizing equation A-5:

$$p_{\text{int}2} = p_{\text{int}1} \frac{\tan \alpha}{\cos \nu}. \quad (\text{A-15})$$

Although this result is derived in the limit of weak anisotropy and small offset, numerical testing shows that it remains valid for arbitrary strength of the anisotropy and the full offset range.

To express the asymmetry attributes as a function of depth beneath the CMP location (z_{CMP}), we simplify equations A-2 and A-3 for the depth z_r of the conversion point using the weak-anisotropy, small-offset approximation:

$$z_r = z_{\text{CMP}} [\cos^2 \nu - (1 + 4\delta)p_{\text{int}1}^2 V_{P0}^2 \sin^2 \nu]. \quad (\text{A-16})$$

The contribution of the P-leg to the time asymmetry can be obtained by substituting equation A-1 into equation 1. We use equa-

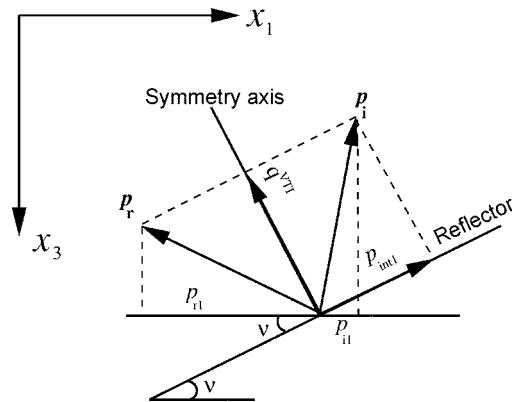


Figure A-1. Geometrical relationships between the slowness components of the incident and reflected P-waves in the dip plane of a TTI layer. The symmetry axis is orthogonal to the dipping interface. p_i and p_r are the slowness vectors of the incident and reflected waves, respectively; p_{i1} and p_{r1} are the horizontal slowness components of the incident and reflected waves. q^{VTI} is the slowness component along the symmetry axis, and $p_{\text{int}1}$ is the slowness projection onto the interface in the dip plane.

tions A-13 and A-14 to find the partial derivatives of the vertical slownesses needed in equation A-1, which yields the traveltime as a function of the slowness components $p_{\text{int}1}$ and $p_{\text{int}2}$ along the interface. Equation A-15 then helps to obtain the time-asymmetry attribute on a line with azimuth α . After further linearization in the parameters ϵ , δ , and the combinations $|p_{\text{int}1}V_{P0}|$ and $|p_{\text{int}2}V_{P0}|$ using symbolic software Mathematica, we find

$$\Delta t_P = 2z_{\text{CMP}}p_{\text{int}1} \sin \nu \left[1 + 2\delta + p_{\text{int}1}^2 V_{P0}^2 (1 + 4\epsilon) \right. \\ \left. \times \left(1 + \frac{\tan^2 \alpha}{\cos^2 \nu} \right) \right]. \quad (\text{A-17})$$

The approximate time asymmetry of the P-leg in equation A-17 is expressed through the slowness $p_{\text{int}1}$, which cannot be estimated directly from surface reflection data. It is more practical to represent the asymmetry through the offset x_{PP} of the reflected PP-wave. Substituting the derivatives of the vertical P-wave slowness q_P into equations A-6 and A-7 and evaluating the result for the slownesses given by equations A-13 and A-14, we obtain the PP-wave offset (x_{PP}) from equation A-4:

$$x_{PP} = p_{\text{int}1} V_{P0} z_{\text{CMP}} \sec \alpha \left[2 + 4\delta + p_{\text{int}1}^2 V_{P0}^2 \right. \\ \left. \times (1 - 4\delta + 8\epsilon) \left(1 + \frac{\tan^2 \alpha}{\cos^2 \nu} \right) \right]. \quad (\text{A-18})$$

Equations A-17 and A-18 cannot be used in the strike direction ($\alpha = 90^\circ$) where $p_{\text{int}1} = 0$. To remove this ambiguity, we replace $p_{\text{int}1}$ with $p_{\text{int}2}$ for $\alpha = 90^\circ$ using equation A-15.

It is convenient to expand Δt_P in a Taylor series in x_{PP} around zero offset:

$$\Delta t_P = \frac{\partial \Delta t_P}{\partial x_{PP}} x_{PP} + \frac{1}{6} \frac{\partial^3 \Delta t_P}{\partial x_{PP}^3} x_{PP}^3 + \dots \quad (\text{A-19})$$

Equation A-19 contains only odd powers of offset because the terms even in x_{PP} do not contribute to the moveout asymmetry. Evaluating the partial derivatives in equation A-19 using the chain rule applied to equations A-17 and A-18, we arrive at

$$\Delta t_P = \frac{\sin \nu \cos \alpha}{V_{P0}} x_{PP} + \frac{(1 - 2\delta) \sin \nu \cos^3 \alpha}{8V_{P0} z_{\text{CMP}}^2} \\ \times \left(1 + \frac{\tan^2 \alpha}{\cos^2 \nu} \right) x_{PP}^3. \quad (\text{A-20})$$

The linearized contribution of the S-leg to the time-asymmetry attribute can be found from the P-wave equation A-20 using the general transformation rule valid in the limit of weak anisotropy (Tsvankin, 2001, p. 26):

$$V_{P0} \rightarrow V_{S0}, \quad \epsilon \rightarrow 0, \quad \delta \rightarrow \sigma; \\ \sigma \equiv \frac{V_{P0}^2}{V_{S0}^2} (\epsilon - \delta).$$

The above substitutions give the following expression for the corresponding S-wave asymmetry component Δt_S :

$$\Delta t_S = \frac{\sin \nu \cos \alpha}{V_{S0}} x_{SS} + \frac{(1 - 2\sigma) \sin \nu \cos^3 \alpha}{8V_{S0} z_{\text{CMP}}^2} \\ \times \left(1 + \frac{\tan^2 \alpha}{\cos^2 \nu} \right) x_{SS}^3. \quad (\text{A-21})$$

Although the common-midpoints for the PP- and SS-waves processed by the PP + PS = SS method are not exactly the same, the difference between the values of z_{CMP} for Δt_P and Δt_S can be ignored if the offsets are sufficiently small. Because of the typically large velocity ratios V_{P0}/V_{S0} , the offsets of the constructed SS-wave seldom exceed the reflector depth, so the term x_{SS}^3 in equation A-21 can be neglected.

The total time-asymmetry attribute of the PS-wave can be found by substituting equations A-20 and A-21 into equation A-1 and taking into account that the contributions of the P- and S-legs should have opposite signs (Part 1):

$$\Delta t_{PS} = \sin \nu \cos \alpha \left(\frac{x_{PP}}{V_{P0}} - \frac{x_{SS}}{V_{S0}} \right) + \frac{(1 - 2\delta) \sin \nu \cos^3 \alpha}{8V_{P0} z_{\text{CMP}}^2} \\ \times \left(1 + \frac{\tan^2 \alpha}{\cos^2 \nu} \right) x_{PP}^3. \quad (\text{A-22})$$

Since the offsets x_{PP} and x_{SS} are related to each other, equation A-22 can be further simplified by expressing x_{PP} through x_{SS} . Applying the transformation P-to-S rule to equation A-18 yields the offset x_{SS} as a function of $p_{\text{int}1}$ and azimuth α :

$$x_{SS} = p_{\text{int}1} V_{S0} z_{\text{CMP}} \sec \alpha \left[2 + 4\sigma \right. \\ \left. + p_{\text{int}1}^2 V_{S0}^2 (1 - 4\sigma) \left(1 + \frac{\tan^2 \alpha}{\cos^2 \nu} \right) \right]. \quad (\text{A-23})$$

Expanding x_{PP} in a cubic Taylor series in x_{SS} around zero offset leads to

$$x_{PP} = \frac{\partial x_{PP}}{\partial x_{SS}} x_{SS} + \frac{1}{2} \frac{\partial^2 x_{PP}}{\partial x_{SS}^2} x_{SS}^2 + \frac{1}{6} \frac{\partial^3 x_{PP}}{\partial x_{SS}^3} x_{SS}^3. \quad (\text{A-24})$$

The derivatives in equation A-24 can be determined from equations A-18 and A-23, which gives the following expression for the PP-wave offset:

$$x_{PP} = \frac{V_{P0}(1 + 2\delta)}{V_{S0}(1 + 2\sigma)} x_{SS} + \frac{(1 - 4\delta + 8\epsilon)V_{P0}^3 \cos^2 \alpha}{8(1 + 2\sigma)^3 V_{S0}^3 z_{\text{CMP}}^2} \\ \times \left(1 + \frac{\tan^2 \alpha}{\cos^2 \nu} \right) x_{SS}^3. \quad (\text{A-25})$$

Formally, in the linearized weak-anisotropy approximation the parameter σ has to be dropped from the denominator of the x_{SS}^3 -term. However, since σ can be relatively large for typical TI formations, keeping it in the denominator increases the accuracy of the approximation for the time asymmetry.

Substituting equation A-25 into equation A-22, we obtain the final expression for the time-asymmetry attribute in terms of the offset x_{SS} :

$$\Delta t_{PS} = \frac{-2 \sin \nu \cos \alpha}{V_{S0}} \chi x_{SS} + \frac{(1 + 4\epsilon)V_{P0}^2 \sin \nu \cos^3 \alpha}{4(1 + 2\sigma)^3 V_{S0}^3 z_{CMP}} \times \left(1 + \frac{\tan^2 \alpha}{\cos^2 \nu}\right) x_{SS}^3, \quad (\text{A-26})$$

where $\chi \equiv (\sigma - \delta)/(1 + 2\sigma)$.

APPENDIX B

APPROXIMATE OFFSET-ASYMMETRY ATTRIBUTE

Here, we apply the approach described in Appendix A to obtain an approximation for the offset-asymmetry attribute of the PSV-wave in a TTI layer. Using equations 2 and A-6, we can write an exact parametric equation for the projection of the offset-asymmetry vector $\Delta \mathbf{x}_{PS}$ onto the x_1 -axis as

$$\Delta x_{1_{PS}} \equiv \Delta x_{1_P} - \Delta x_{1_S} = z_r [q_{P_i} + q_{P_r} - (q_{S_i} + q_{S_r})], \quad (\text{B-1})$$

where q is the vertical slowness, $q_{P_i} \equiv \partial q_P / \partial P_i$, $q_{P_r} \equiv \partial q_P / \partial P_r$, $q_{S_i} \equiv \partial q_S / \partial S_i$, and $q_{S_r} \equiv \partial q_S / \partial S_r$; P_i and P_r are the horizontal slownesses for the incident and reflected legs of the P-wave, and S_i and S_r are the same quantities for the S-wave. The slowness vectors are related to each other by Snell's law at the reflection point.

To express the P-wave component of $\Delta x_{1_{PS}}$ as a function of the slowness projection onto the interface in the dip plane (p_{int1}), we evaluate the derivatives of the vertical slowness from Appendix A using equations A-13 and A-14 derived in the weak-anisotropy, small-offset limit:

$$\begin{aligned} \Delta x_{1_P} &= z_r (q_{P_i} + q_{P_r}) \\ &= z_r \sec^2 \nu \tan \nu [1 + 2(1 + 4\delta)p_{int1}^2 V_{P0}^2 + \cos 2\nu]. \end{aligned} \quad (\text{B-2})$$

It is of interest that equation B-2 is independent of p_{int2} . The transformation rule gives the corresponding equation for the S-wave:

$$\Delta x_{1_S} = z_r \sec^2 \nu \tan \nu [1 + 2(1 + 4\sigma)p_{int1}^2 V_{S0}^2 + \cos 2\nu]. \quad (\text{B-3})$$

Substituting the P- and S-wave asymmetry contributions from equations B-2 and B-3 into equation B-1 yields

$$\Delta x_{1_{PS}} = 2z_r p_{int1}^2 \sec^2 \nu \tan \nu [(1 + 4\delta)V_{P0}^2 - (1 + 4\sigma)V_{S0}^2]. \quad (\text{B-4})$$

Expressing the depth of the reflection point z_r in terms of z_{CMP} using equation A-16, we obtain

$$\Delta x_{1_{PS}} = 2z_{CMP} p_{int1}^2 \tan \nu [(1 + 4\delta)V_{P0}^2 - (1 + 4\sigma)V_{S0}^2]. \quad (\text{B-5})$$

To find $\Delta x_{1_{PS}}$ as a function of the SS-wave offset x_{SS} , we substitute p_{int1} from equation A-23:

$$\Delta x_{1_{PS}} = \frac{\tan \nu}{2z_{CMP}} \left[\frac{(1 + 4\delta)V_{P0}^2}{(1 + 4\sigma)V_{S0}^2} - 1 \right] x_{SS}^2 \cos^2 \alpha. \quad (\text{B-6})$$

The magnitude x_{PS} of the offset-asymmetry vector for any azimuth α can be obtained by combining equations A-4 and A-5:

$$\Delta x_{PS} = \frac{\Delta x_{1_{PS}}}{\cos \alpha}. \quad (\text{B-7})$$

Substituting equation B-6 into equation B-7 yields

$$\Delta x_{PS} = \frac{\tan \nu}{2z_{CMP}} \left[\frac{(1 + 4\delta)V_{P0}^2}{(1 + 4\sigma)V_{S0}^2} - 1 \right] x_{SS}^2 \cos \alpha. \quad (\text{B-8})$$

In the presence of moveout asymmetry, the minimum traveltime of PS-waves in a CMP gather occurs at nonzero offset. As discussed in Part 1 and Tsvankin (2001, Appendix 5B), the offset $x_{min}(\alpha)$ of the traveltime minimum corresponds to the PS ray for which the projections of the slowness vectors for the P- and S-legs onto the CMP line are equal to each other. The dip component of the slowness projection onto the interface can be found in the limit of weak anisotropy, small offset, and small dip as

$$p_{int1}^{min} = \frac{\sin \nu \cos^2 \alpha}{2} \left(\frac{1}{V_{S0}} - \frac{1}{V_{P0}} \right). \quad (\text{B-9})$$

Equation B-9 contains no contribution of the anisotropic parameters and coincides with the expression for p_{int1}^{min} for isotropic or VTI media given in Tsvankin (2001, Appendix 5D.2).

Evaluating the derivatives of the vertical slowness (see Appendix A) at p_{int1}^{min} and substituting the result into equations A-4, A-6, and A-7, we find the azimuthally varying offset of the traveltime minimum:

$$\begin{aligned} x_{min}(\alpha) &= \frac{z_{CMP}}{2 \cos \nu} \left[\frac{\sin \nu}{V_{P0}} - \frac{\sin \nu}{V_{S0}} \right] \\ &\times [V_{P0}(1 + 2\delta) + V_{S0}(1 + 2\sigma)] \cos \alpha. \end{aligned} \quad (\text{B-10})$$

REFERENCES

- Dewangan, P., and I. Tsvankin, 2006a, Modeling and inversion of PS-wave moveout asymmetry for tilted TI media: Part 1 — Horizontal TTI layer: *Geophysics*, this issue.
- , 2006b, Velocity-independent layer stripping of PP and PS reflection traveltimes: *Geophysics*, this issue.
- Grechka, V., and P. Dewangan, 2003, Generation and processing of pseudo shear-wave data: Theory and case study: *Geophysics*, **68**, 1807–1816.
- Grechka, V., and I. Tsvankin, 1999, 3-D moveout inversion in azimuthally anisotropic media with lateral velocity variation: Theory and a case study: *Geophysics*, **64**, 1202–1218.
- , 2000, Inversion of azimuthally dependent NMO velocity in transversely isotropic media with a tilted axis of symmetry: *Geophysics*, **65**, 232–246.
- , 2002, PP + PS = SS: *Geophysics*, **67**, 1961–1971.
- Grechka, V., A. Pech, and I. Tsvankin, 2002, Multicomponent stacking-velocity tomography for transversely isotropic media: *Geophysics*, **67**, 1564–1574.
- Grechka, V., A. Pech, I. Tsvankin, and B. Han, 2001, Velocity analysis for tilted transversely isotropic media: A physical-modeling example: *Geophysics*, **66**, 904–910.
- Isaac, J. H., and D. C. Lawton, 1999, Image mispositioning due to dipping TI media: A physical seismic modeling study: *Geophysics*, **64**, 1230–1238.
- Lawton, D. C., J. H. Isaac, R. W. Vestrum, and J. M. Leslie, 2001, Slip-sliding away - some practical implications of seismic velocity anisotropy on depth imaging: *The Leading Edge*, **20**, 70–73.
- Thomsen, L., 1986, Weak elastic anisotropy: *Geophysics*, **51**, 1954–1966.
- Tsvankin, I., 1995, Normal moveout from dipping reflectors in anisotropic media: *Geophysics*, **60**, 268–284.

———, 2001, Seismic signatures and analysis of reflection data in anisotropic media: Elsevier Science Publishing Company.

Tsvankin, I., and V. Grechka, 2000, Dip moveout of converted waves and parameter estimation in transversely isotropic media: *Geophysical Prospecting*, **48**, 257–292.

———, 2002, 3D description and inversion of reflection moveout of PS-waves in anisotropic media: *Geophysical Prospecting*, **50**, 301–316.

Vestrum, R. W., D. C. Lawton, and R. Schmid, 1999, Imaging structures below dipping TI media: *Geophysics*, **64**, 1239–1246.